Physics of Fluids

RESEARCH ARTICLE | DECEMBER 05 2025

Assessing the effects of viaduct configurations on traffic pollutant transport: A large-eddy simulation study comparing quasi-two-dimensional and three-dimensional urban canyons

Lemei Li (李乐梅) ; Bin Lu (陆斌) ; Peng Qin (秦鹏) ; Lili Xia (夏丽丽) ; Jun Cai (蔡军) ; Jing Dong (董菁) ; Pengyuan Shen (沈鹏元) ; Huanhuan Wang (王欢欢) ; Zhen Han (韩臻) ; Guangdong Duan (段广东) ; Dengkai Chi (迟登凯) ; Yunfei Fu (付云飞) ; Qiusheng Li (李秋胜) ; Xing Zheng (郑星) ✉

Physics of Fluids 37, 125127 (2025)
https://doi.org/10.1063/5.0303918

Physics of Fluids ARTICLE pubs.aip.org/aip/pof

Assessing the effects of viaduct configurations on traffic pollutant transport: A large-eddy simulation study comparing quasi-two-dimensional and three-dimensional urban canyons

Cite as: Phys. Fluids **37**, 125127 (2025); doi: 10.1063/5.0303918
Submitted: 25 September 2025 · Accepted: 11 November 2025 ·
Published Online: 5 December 2025

Lemei Li (李乐梅),[1,2] Bin Lu (陆斌),[1] Peng Qin (秦鹏),[3] Lili Xia (夏丽丽),[3] Jun Cai (蔡军),[2] Jing Dong (董菁),[2] Pengyuan Shen (沈鹏元),[4] Huanhuan Wang (王欢欢),[5] Zhen Han (韩臻),[6] Guangdong Duan (段广东),[7] Dengkai Chi (迟登凯),[8] Yunfei Fu (付云飞),[9] Qiusheng Li (李秋胜),[1] and Xing Zheng (郑星)[1,a)]

AFFILIATIONS

[1]Department of Architecture and Civil Engineering, City University of Hong Kong, Hong Kong SAR, China
[2]School of Architecture and Fine Art, Dalian University of Technology, Dalian, China
[3]Building Physics and Services, Department of the Built Environment, Eindhoven University of Technology, Eindhoven, The Netherlands
[4]Tsinghua Shenzhen International Graduate School, Tsinghua University, Shenzhen, China
[5]School of Civil and Environmental Engineering, Cornell University, Ithaca, New York 14853, USA
[6]Department of Architecture, Tianjin University, Tianjin, China
[7]School of Energy and Environment, Key Laboratory of Clean Energy, Shenyang Aerospace University, Shenyang, China
[8]Future Cities Laboratory Global, Singapore-ETH Centre, Singapore
[9]Department of Civil and Environmental Engineering, The Hong Kong University of Science and Technology, Hong Kong SAR, China

[a)]**Author to whom correspondence should be addressed:** x.zheng@cityu.edu.hk

ABSTRACT

Viaducts are widely used across high-density urban environments. Although their influence on pollutant dispersion has been studied, the majority of studies use quasi-two-dimensional (quasi-2D) street canyon models, with few directly comparing them to three-dimensional (3D) ones. This study explores these differences by conducting large-eddy simulations using both quasi-2D and 3D models to assess traffic pollutant dispersion in street canyons with urban viaduct configurations under perpendicular approaching wind. Four configurations are examined, including ground-level roads only, viaducts without noise barriers, and viaducts with bilateral noise barriers of 2 or 4 m in height. Five important parameters, including mean wind velocity, pollutant concentration, indoor personal intake fraction (P_{IF}), vertical mass fluxes, and pollutant exchange velocity, are employed to evaluate the differences between quasi-2D and 3D models. The findings show that quasi-2D models with various viaduct configurations yield mean indoor P_{IF} for buildings away from the road and overall street canyon pollutant concentrations comparable to those from 3D models. However, quasi-2D models with viaduct configurations tend to overestimate spatially averaged pollutant concentrations at pedestrian-level zones by up to 1.8 times and overestimate mean indoor P_{IF} in near-road buildings by as much as 54.8% compared to the 3D cases with viaduct configurations being investigated. Moreover, 3D models with viaduct configurations exhibit better pollutant removal efficiency, with the dimensionless pollutant exchange velocity through the roof level up to 33.6% higher than in quasi-2D models.

I. INTRODUCTION

Street canyons are narrow urban spaces lined with buildings on both sides and form distinct microclimatic environments that significantly influence local air quality. Within these canyons, traffic emissions can accumulate, posing health risks to pedestrians and residents living near the roads.[1–3] In recent years, urban viaducts have been widely introduced in street canyons to improve transportation efficiency, particularly in densely populated residential areas. These viaducts are often accompanied by noise barriers, resulting in a built environment that differs from traditional street canyons. The street

canyons with the viaducts present new environmental challenges (e.g., limited ventilation, pollutant accumulation) due to their modified geometry and the altered placement of emission source locations within them. Specifically, viaducts can alter the pollutant spatial distribution in street canyons, shifting zones of high concentration from ground level to elevated positions, particularly around the viaduct deck.[4–6] Noise barriers installed on viaducts generally further impede pollutant dispersion in viaduct regions, increasing the on-road pollutant concentrations.[5,7] The viaducts and their noise barriers also affect indoor air quality. Viaducts can reduce area-averaged indoor pollutant concentrations.[7] Noise barriers can also slightly reduce traffic-related indoor pollutant exposure in buildings adjacent to roads.[5,6] Therefore, understanding the flow and pollutant transport mechanisms in canyons with viaducts and noise barriers is critical for evaluating residents' exposure to traffic-related pollutants and for informing mitigation strategies in near-road neighborhood design.

Over the past decades, computational fluid dynamics (CFD) simulations have been extensively employed to estimate the pollutant distribution across various urban environments (e.g., Refs. 8–11). Likely, CFD simulations have also been widely used to explore how viaducts and noise barriers influence the dispersion of traffic-related pollutants in street canyons, as summarized in Table I. These studies have demonstrated that pollutant dispersion and airflow patterns within street canyons can be influenced by their geometric parameters. These key geometric parameters include the street length (L),[12,13] street canyon aspect ratio (H/W),[6] viaduct height and width,[14] noise barrier height,[15] and building height variability.[16] In addition, the effects of viaduct and noise barriers on transport of traffic-related pollutants in street canyons under different ground heating intensities have also been explored, e.g., by Hang *et al.*[7,17] It is worth noting that when the approaching wind is perpendicular to the long axis of a street canyon, pollutants tend to accumulate most within the street canyon compared to other wind directions.[18,19] Therefore, all studies in Table I adopted this perpendicular wind direction scenario to investigate the most unfavorable pollution dispersion in street canyons.

In CFD simulations, street canyons are typically idealized as either two-dimensional (2D) or three-dimensional (3D) configurations. The 2D street canyon models assume infinitely long and continuous buildings along the street's longitudinal axis. There are two types of 2D street canyon models in previous CFD studies: pure 2D (solves fluid flow in two dimensions) [see Fig. 1(a)] and quasi-2D (solves fluid

TABLE I. Non-exhaustive overview of CFD studies focusing on the impacts of street canyons with viaduct configurations on pollutant dispersion over the past decade. "P" indicates the approaching flow is perpendicular to the canyon's long axis. "H_1" and "H_2" represent the leeward building's height and windward building's height, respectively. When $H_1 = H_2$, the common building height is denoted by "H." "W" and "L" stand for the street canyon's width and length, respectively. P_{IF} denotes the personal intake fraction. $C_{outdoor}$ and C_{indoor} represent outdoor and indoor pollutant concentrations, respectively. The symbol "∞" signifies an infinitely long street canyon (L), whereas "…" marks missing information.

Ref.	CFD	Quasi-2D/3D	H/W	L/H	Wind direction	Viaduct width (m)	Viaduct height (m)	Noise barriers height (m)	Target parameters
4	RANS	Quasi-2D	1, 3, 5	∞	P	16	9	4	P_{IF}
5	RANS	Quasi-2D	1, 1.5, 2	∞	P	16	9	2, 4	Indoor daily pollutant exposure, P_{IF}
6	RANS	Quasi-2D	1–6	∞	P	16	9	4	Indoor daily pollutant exposure, P_{IF}
7	RANS	Quasi-2D	1	∞	P	14	7.8	2.3, 4.3	C_{indoor}, $C_{outdoor}$
14	RANS	Quasi-2D	0.5, 0.67, 1	∞	P	10	8–12	2.5	$C_{outdoor}$
15	RANS	Quasi-2D	1	∞	P	16	8	2–8	$C_{outdoor}$
16	RANS	Quasi-2D	1/3, (H_1/H_2 from 1/1 to 6/5)	∞	P	20	10	4	$C_{outdoor}$
17	RANS	Quasi-2D	1	∞	P	14	7.8	None	C_{indoor}, $C_{outdoor}$
20	RANS	3D	0.5, 1, 1.5	1	P	15	7	4	P_{IF}, $C_{outdoor}$
21	RANS	Quasi-2D	1	∞	P	8, 10, 12, 14	8–20	None	$C_{outdoor}$
22	RANS	Quasi-2D	1.5	∞	P	17	8	…	$C_{outdoor}$
23	RANS	Quasi-2D	2	∞	P	16	9	1, 2, 3	$C_{outdoor}$
24	RANS	Quasi-2D	1	∞	P	8–18	5–15	None	$C_{outdoor}$, Mean particle residence time
25	RANS	Quasi-2D	$H_1/W = 0$, $H_2/W = 2$	∞	P	34	2.4	0.3	$C_{outdoor}$
26	RANS	Quasi-2D	1	∞	P	10	3.2–14	None	Turbulent kinetic energy, $C_{outdoor}$
27	RANS	Quasi-2D	1	∞	P	20, 30, 40	15–60	None	$C_{outdoor}$
28	RANS and LES	3D	1	10	P	9	9, 13.5, 18	None	$C_{outdoor}$
29	LES	3D	1, 2, 3		P	4, 8, 12	0, 1.1, 3	1.1, 3	Gust and mean wind velocity
30	LES	3D	1	3	P	4	8	3	Turbulent momentum flux, $C_{outdoor}$

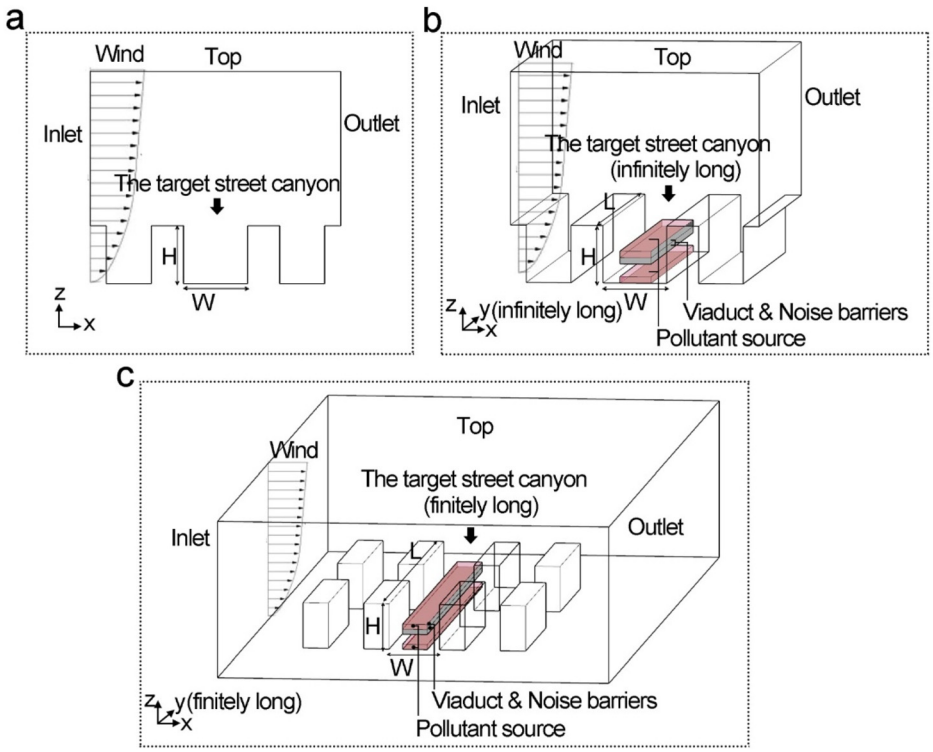

FIG. 1. The typical configurations of computational domains for street canyons in CFD simulations: (a) the pure 2D model, (b) the quasi-2D model, (c) the 3D model.

flow in all three dimensions for a quasi-infinitely long street canyon using lateral periodic boundary conditions) [see Fig. 1(b)]. The pure 2D model was primarily adopted in early studies to investigate basic ventilation and pollutant diffusion patterns in isolated street canyons.[31] With improvements in computational techniques, pure 2D models have not been used in the past decade for studying how viaducts configurations affect pollutant dispersion and have been replaced by quasi-2D models, as summarized in Table I. CFD studies with quasi-2D models show that the canyon aspect ratio (H/W) can significantly affect the wind flow characteristics inside street canyons (e.g., Ref. 32). Many such studies also indicate that the viaduct can be considered as an extra horizontal surface, which decreases the canyon's effective aspect ratio.[4–6] These studies further point out that the presence of viaduct configurations affect flow patterns and pollutant transport in regular quasi-2D canyons ($H/W = 0.5$–1) to a greater extent than in deep canyons ($H/W = 5$–6).

In contrast, CFD studies with 3D street canyon models typically represent the urban environment as a series of cuboid blocks with spacing, capturing more realistic street layouts [see Fig. 1(c)]. A key advantage of these 3D models is their ability to assess the influence of another important parameter—street length (L). Michioka *et al.*[33] used large-eddy simulations (LES) to estimate pollutant removal in canyons with various L/H ratios (1, 2, 4, 8, and ∞). They found that pollutant concentration increases with L/H, while the proportion of turbulent mass flux in the mean net flux at roof level decreases when L/H is changed from 2 to 8. Interestingly, this value approaches unity when $L/H = 1$ or ∞.

Compared to the 3D street canyon models, quasi-2D models have been more commonly employed to examine how urban viaduct configurations influence pollutant dispersion within street canyons, as summarized in Table I. This preference is mainly because quasi-2D models require far less computational cost than 3D models. However, it is known that 3D models generally offer a more realistic representation of complex urban environments and can provide more practical guidance for urban road design. Meanwhile, several CFD studies have reported the significant differences in airflow patterns and pollutant concentrations between quasi-2D and 3D street canyon models (e.g., Refs. 20 and 34). For instance, Hang *et al.*[20] reported significant lateral pollutant transport occurring at building gaps in 3D canyons with viaduct configurations. This transport mechanism contrasts with that of quasi-2D configurations, where pollutant removal is limited to vertical dispersion across the canyon roof. In addition, their study found that quasi-2D models of street canyons with viaducts tended to overestimate traffic pollutant exposure for residents, with the personal intake fraction (P_{IF}) in 3D models being an order of magnitude lower than in quasi-2D models. This discrepancy may stem from critical 3D model configurations (such as intersections and building gaps, which define the effective street length) that are typically neglected in quasi-2D models. Specifically, in relatively short canyons, corner vortices can become sufficiently intense to inhibit the development of a dominant vortex-oriented perpendicular to the street canyon in the central region. As the street length increases, the influence of the corner vortices on the dominant vortex diminishes. Mei *et al.*[34] concluded that a regular 3D street canyon ($H/W = 1$) can be simplified and examined as a 2D canyon in CFD simulations when the street canyon is sufficiently long ($L/W > 20$). However, such analyses were performed using steady Reynolds-averaged Navier–Stokes (RANS) simulations, which only capture time-averaged pollutant distributions and flow patterns

and cannot reproduce the transient features of turbulent diffusion accurately.[35–37] Additionally, past studies have shown that RANS has a deficiency in accurately reproducing the secondary vortices generated by urban or building geometrical details. Therefore, it is essential to understand the extent to which LES simulations using quasi-2D and 3D street canyon models with viaducts differ in their representation of pollutant dispersion. To the best of the authors' knowledge, the differences in airflow patterns and pollutant dispersion between quasi-2D and 3D street canyons with viaducts remain unclear. This study aims to address this knowledge gap by conducting a series of LES-based CFD simulations to compare quasi-2D and 3D street canyon models in terms of wind flow fields, traffic pollutant dispersion, and traffic pollutant exposure for residents. The simulations are carried out under the perpendicular wind condition, using three typical viaduct configurations and one no-viaduct street canyon configuration. The LES-based CFD simulations enable a high-fidelity assessment of how viaduct-induced flow separation and transient features influence near-road pollutant dispersion. Therefore, this study extends previous RANS-based findings on the differences between quasi-2D and 3D street canyon models and further encompasses a broader range of canyon configurations, including those with viaduct structures.

The structure of the rest of this paper is as follows: Sec. II shows the numerical setups for LES simulations, pollutant dispersion modeling, and target indicators. Section III reports the differences between quasi-2D and 3D LES results, Sec. IV discusses the findings, highlights study limitations, and offers suggestions for future studies. Finally, Sec. V presents the conclusion.

II. METHODOLOGY

This study employs LES-based CFD simulations to explore traffic pollutant dispersion in street canyons under various viaduct configurations. The LES approach has been widely acknowledged for its capability to accurately capture turbulent pollutant transport processes,[36,38–40] and its accuracy has been validated through comparison with wind tunnel experiments, as described in supplementary material S1.[41,42] Table II presents the results of validation metrics [mean absolute error (MAE) and root mean square error (RMSE)] for dimensionless mean pollutant concentration of LES-based CFD simulations compared to the wind tunnel experiment. Further methodological details, including grid independence assessments and model validation, are available in the previous work.[2,43]

A. Studied cases

The quasi-2D and 3D street canyon models considering viaducts used for LES simulations are first introduced in this section. As shown in Fig. 2(a), the 3D model consists of an 8-row × 16-column array of buildings with multiple stories. These buildings surround four separate street canyons. Each building has a height (H) of 18 m, a length of 34 m, and a depth of 10 m. The street width (W) and the lateral spacing between buildings are both 20 m, resulting in a H/W of 0.9. The designated target zone, located in the upstream street canyon, measuring 88×64 m^2, and contains six buildings labeled B7 to B12. This zone is selected to enable direct comparison with the quasi-2D model while avoiding significant disturbances in airflow and pollutant accumulation caused by road intersections. Among these buildings, B7 to B10 are directly adjacent to the roadside, while B11 and B12 are the buildings away from the road within the residential area [shown in Fig. 2(a)]. These two groups of buildings are supposed to be affected more by traffic pollutant emissions, compared to the other buildings in the residential area. In the corresponding quasi-2D model, shown in Fig. 2(b), 16 multi-story buildings are arranged along the streamwise wind direction with two street canyons located between L4 and L5, and L12 and L13, respectively. Each building is also 18 m in height and has a length of 90 m, and a depth of 10 m. The street width remains 20 m, yielding the same H/W as the 3D model. The target zone in the quasi-2D model, located in the upstream street canyon, measures 90 m ($= 5H$) in length and 64 m in width, and contains three buildings labeled L4 to L6. These buildings correspond to the 3D model as follows: L4 corresponds to buildings B7 and B8, L5 to B9 and B10, and L6 to B11 and B12. Note that the spatial coordinate system in both quasi-2D and 3D models is defined such that the streamwise direction is indicated by the x-axis, the spanwise direction by the y axis, and the vertical direction the z axis.

The quasi-2D and 3D street canyon models employ the same viaduct and ground-level road configurations. Four representative configurations are examined and depicted in Fig. 2(c):

(1) no viaduct—only 16 m wide ground-level roads (case NV);
(2) viaduct with no noise barriers—both the viaduct-level and ground-level roads are 8 m wide (case Vb0);
(3) viaduct with bilateral noise barriers of 2 m in height—both the viaduct-level and ground-level roads are 8 m wide (case Vb2);
(4) viaduct with bilateral noise barriers of 4 m in height—both the viaduct-level and ground-level roads are 8 m wide (case Vb4).

The subscripts "2d" and "3d" are added to the case names in the following text to distinguish whether the case is a quasi-2D or 3D model. In the no-viaduct scenario, the ground-level road consists of four lanes (each assumed to be 4 m wide), whereas in scenarios with a viaduct, both the ground-level and viaduct-level roads comprise two lanes each. This setup keeps the road area consistent across all configurations. The viaduct features a clearance height (6 m) to the deck underside. Regarding the viaduct configuration elements, only the viaduct deck (2 m thick) and noise barriers (with no thickness) are modeled in this study. Other structural elements, including supporting

TABLE II. Validation metrics (MAE and RMSE) for dimensionless mean pollutant concentration (C^+) over the leeward and windward walls between the LES simulation and the wind tunnel experiment.

	C^+ along four vertical lines near the leeward wall				C^+ along four vertical lines near the windward wall			
Validation metrics	y/H = −4.92	y/H = −3.75	y/H = −1.25	y/H = 0	y/H = −4.92	y/H = −3.75	y/H = −1.25	y/H = 0
MAE	1.38	3.37	1.50	1.46	1.07	1.01	0.14	0.53
RMSE	1.57	3.44	1.77	1.56	1.12	1.01	0.15	0.67

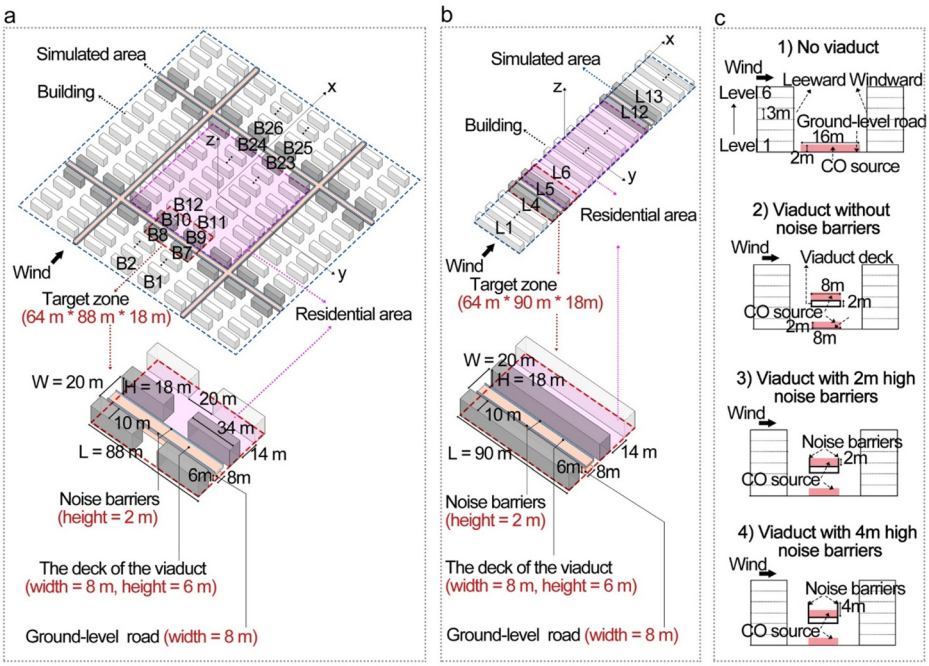

FIG. 2. Perspective illustration of the modeled buildings, viaduct, and noise barriers for case Vb0 in (a) the 3D model and (b) the quasi-2D model; (c) cross-sectional views of the four studied configurations.

pillars, are excluded, consistent with the approach adopted in previous studies.[14,16,28] Although vehicle movement can influence local pollutant distribution near vehicles,[44–46] previous studies demonstrated that, under wind-dominated conditions, two-way traffic exerts only a minor effect on overall roadside pollutant concentrations.[18,47] Since the present analysis assumes a two-lane or four-lane road configuration in a two-way direction, the effect of moving vehicles is not considered. The approaching wind is perpendicular to the building's long side.

B. Computational domain and grids

Figure 3(a) shows the computational domain used in the 3D street canyon model with viaducts and 2- m-high noise barriers (case $Vb2_{3d}$) for LES simulations under a perpendicular wind condition. The domain extends 5*H* upstream and 10*H* downstream from the simulated area, with a vertical height of 6H.[48] Figure 3(b) presents the computational domain used in the quasi-2D street canyon model with case $Vb2_{2d}$ for LES simulations. The same upstream and downstream lengths as the 3D street canyon model are applied. The domain height is set to 7.5*H* following the established best practices guidelines for quasi-2D canyon simulations.[48]

The grid resolution and structure are consistent with the grid sensitivity analysis in supplement material S1. The grid arrangement is identical in both the quasi-2D and 3D models across the entire domain. A non-conformal grid is employed because it reduces the total number of grids while maintaining sufficient resolution in the target zone. The computational domain is subdivided into three nested subdomains—D_1, D_2, and D_3—from the innermost to the outermost. The grids are successively refined with a ratio of 1:2 from D_1 to D_2 and from D_2 to D_3 [see Figs. 3(a) and 3(b)].[49] Sub-domain D_1 is composed of cubic grids with edge lengths of $D_x = D_y = D_z = W/40$. Horizontally, it extends 12 m from the residential area boundary and vertically 4 m above the rooftops. Sub-domain D_2 also employs cubic grids, each measuring $D_x = D_y = D_z = W/20$. Sub-domain D_3 contains hexahedral grids gradually stretched in all directions with a ratio of 1.05, except along the interface with D_2, where no stretching is applied to maintain consistency with the mesh resolution of D_2. In total, the 3D computational domain contains approximately 17×10^6 cells, while the quasi-2D computational domain includes around 2.2×10^6 cells.

C. Boundary conditions

Table III summarizes the boundary conditions employed in both quasi-2D and 3D models. A velocity inlet condition is specified at the inlet boundary. To simulate a neutral atmospheric boundary layer, the vertical profiles of mean wind velocity (U), turbulent kinetic energy (k), and turbulence dissipation rate (ε) are specified according to the formulations given in Eqs. (1)–(3):[51] where the ABL friction velocity, $u*_{ABL}$, is prescribed as 0.475 m/s, with von Kármán constant (κ) is set to 0.41. z_0 is specified as 0.3 m as the aerodynamic roughness length, with z representing the vertical height. C_μ is an empirical parameter, set to 0.09. U_{ref}, the reference wind velocity measured 10 m above ground, is 4 m/s. Inflow wind velocity fluctuations are modeled using Sergent's vortex method,[50] with validation reported in prior LES studies.[52,53] N_v (representing the number of vortices) employed in this simulation is calculated using the formula $N_v = N_{in}/4$. In this expression, N_{in} represents the grid number on the inlet plane.[54] In the 3D model, N_v is set to 2457, whereas in the quasi-2D model, it is assigned a value of 244. In the 3D models, symmetry conditions are imposed on the top and side boundaries to maintain a zero normal gradient, whereas in the quasi-2D models, periodic boundary conditions are applied to the side boundaries to represent infinitely long street canyons. No-slip wall conditions are enforced on building facades, viaduct deck, noise

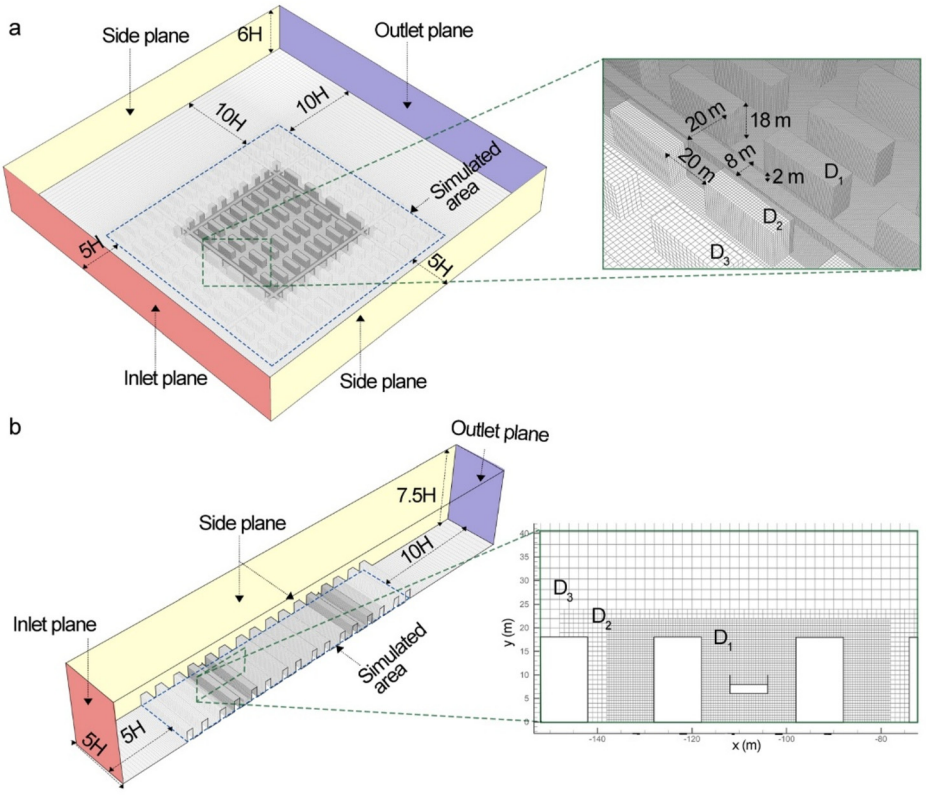

FIG. 3. Boundary conditions, computational domain, and details of grids near buildings in the target zone for case Vb2 under perpendicular wind in (a) the 3D model and (b) the quasi-2D model.

barrier surfaces, and the ground. Near-wall treatment adopt Werner-Wengle wall functions.[55] Zero-gauge pressure condition is applied at the outlet boundary. Carbon monoxide (CO) is chosen as the tracer pollutant owing to its inert nature and consistent application in previous research.[5,6,16,17,20] Its molecular weight is 28.01 g/mol. The pollutant source is modeled as a volumetric release originating from the road region, which corresponds to the red zone in Fig. 2(c). The volumetric source extends 2 m vertically above the ground and the viaduct deck, with its length and width matching the dimensions of the road. Taking into account typical road emission rates and lane widths,[56] the pollutant emission rate is specified as 0.000 416 g/m^{2}s per unit road area.

D. Pollutant dispersion modeling

For the LES simulations of both quasi-2D and 3D street canyon models, a sub-grid-scale (SGS) model is required to represent the effects of unresolved turbulent motions. In this study, the wall-adapting local eddy-viscosity (WALE) model is employed for this purpose, with the constant parameter set to $C_{wale} = 0.325$.[57] The WALE SGS model has demonstrated reliability and has been effectively utilized in earlier research investigating pollutant transport in urban environments.[36,57]

The instantaneous pollutant concentration is treated as a scalar quantity. Its evolution is governed by the Eulerian advection–diffusion equation. The mean (time-averaged) convective mass flux ($Q_{c,i}$) represents pollutant transport driven by the mean flow and is expressed as

$$Q_{c,i} = \langle \overline{u_i} \rangle \langle \overline{c} \rangle, \tag{4}$$

where i denotes the coordinate direction. The overbar represents the filtering operation, while the angle brackets denote the time averaging operator. The total mean turbulent mass flux, $Q_{t,i}$, can be expressed as

$$Q_{t,i} = \left\langle \overline{u_i' c'} \right\rangle + \langle q_{SGS,i} \rangle, \tag{5}$$

where u_i' and c' denote the fluctuating components of velocity and pollutant concentration, respectively. q_{SGS} corresponds to the sub-grid-scale (SGS) mass flux. This term captures the contribution of small-scale turbulent eddies that cannot be directly resolved on the larger-scale pollutant transport. A gradient-diffusion approximation is used to model the instantaneous SGS mass flux. This approach is based on the resolved concentration field and is formulated as

$$q_{SGS,i} = \overline{u_i c} - \overline{u_i}\,\overline{c} = -D_{SGS} \frac{\partial \overline{c}}{\partial x_i}, \tag{6}$$

where u_i represents the instantaneous velocity components. c denotes the instantaneous CO concentration. Calculated as the ratio of the SGS viscosity (ν_{SGS}) to the SGS Schmidt number (Sc_{SGS}), D_{SGS} represents the SGS mass diffusivity [Eq. (7)]. Consistent with established practices in prior research,[58,59] a Schmidt number of 0.7 is applied in the simulation

$$Sc_{SGS} = \frac{\nu_{SGS}}{D_{SGS}}. \tag{7}$$

TABLE III. Boundary conditions in both quasi-2D and 3D models.

Boundary	Quasi-2D/3D	Settings
Inlet plane	Quasi-2D and 3D	Velocity inlet with vortex method $U(z) = \frac{u^*_{ABL}}{\kappa} ln\left(\frac{z+z_0}{z_0}\right)$ (1) $k(z) = \frac{(u^*_{ABL})^2}{\sqrt{C_\mu}}$ (2) $\varepsilon(z) = \frac{(u^*_{ABL})^3}{\kappa(z+z_0)}$ (3)
Outlet plane	Quasi-2D and 3D	Pressure-outlet (static gage pressure = 0 Pa)
Top plane	Quasi-2D and 3D	Symmetry
Side plane	Quasi-2D	Periodic
	3D	Symmetry
Viaduct and noise barrier surfaces and building and ground	Quasi-2D and 3D	No-slip wall (Werner–Wengle wall functions)
Pollutant source	Quasi-2D and 3D	Volumetric source (CO) = 0.000 208 g/m^{3}s, corresponding to the emission rate per unit road area 0.000 416 g/m^{2}s

E. Numerical setups

Prior to data sampling, an initialization phase of 1440 s is conducted for the LES simulations of both quasi-2D and 3D street canyon models. This corresponds to 30 000 time steps, with each time step equal to 0.048 s. The initialization period is equivalent to approximately eight flow-through times ($T_{ft} = L_s/U_{ref}$, with L_s representing the streamwise domain length). During this period, the fluctuations of dimensionless velocity (U/U_{ref}) and dimensionless pollutant concentration (C^+) were observed to diminish significantly after about 30 000 time steps in both quasi-2D and 3D street canyon models, demonstrating that the flow field had achieved statistical convergence. This initialization phase guarantees that all sampled flow variables develop independently of the nonphysical initial conditions.[60] Following the initialization phase, flow and pollutant concentration data are collected and time-averaged over a period of 4320 (around $24T_{ft}$). All these simulations were conducted using the commercial CFD software ANSYS Fluent 2019 R3. Other simulation settings in both quasi-2D and 3D models can be found in Table IV.

F. Target indicators

The following five target indicators are assessed in both quasi-2D and 3D models:

- Mean wind velocity field:
  To allow direct comparison between different cases, the mean wind velocity is expressed in dimensionless form by taking the ratio of the local mean wind velocity (U) to the reference wind velocity (U_{ref}), denoted as U/U_{ref}. The reference velocity is specified as 4 m/s measured 10 m above the ground.
- Mean pollutant concentration field:
  The dimensionless mean pollutant concentration (C^+) is expressed as follows:

$$C^+ = \frac{CU_{ref}H}{Q/l}, \quad (8)$$

TABLE IV. Solver settings.

Item	Settings
Pressure–velocity coupling	SIMPLEC
Spatial discretization	Pressure: second order Momentum: bounded central differencing Concentration: second-order upwind Energy: second-order upwind
Transient formulation	Fraction step
Sub-grid-scale model	WALE SGS model with constant $C_{wale} = 0.325$ and $Sc_{SGS} = 0.7$
Data sampling frequency	Every time step
CFD software	ANSYS Fluent 2019 R3

where $H = 18$ m denotes the height from the ground to the building roof (i.e., the building height). The tracer gas (CO) emission rate per unit length, Q/l, is specified as 0.01 g·s^{-1}m^{-1}.

- Mean mass flux:
To assess pollutant transport across the canyon rooftop (i.e., the top horizontal surface), this study examines the dimensionless mean vertical convective mass flux ($Q_{c,z}/Q_0$) as well as the vertical turbulent mass flux ($Q_{t,z}/Q_0$) of the tracer gas. The reference mass flux Q_0 (g/m^{2}s) is specified as

$$Q_0 = (Q/l)/H. \tag{9}$$

- Mean pollutant exchange velocity:
The dimensionless mean pollutant exchange velocity (U_e/U_{ref}) serves as a key indicator for evaluating the actual efficiency of pollutant removal from street canyons. U_e (m/s) is composed of two contributions:[61,62] a convective component and a turbulent component, which correspond to the first and second terms in Eq. (10), respectively:

$$U_e = U_{e,c} + U_{e,t} = \frac{\int_A Q_{c,z}\,dA}{A[C]} + \frac{\int_A Q_{t,z}\,dA}{A[C]}, \tag{10}$$

where $Q_{c,z}$ and $Q_{t,z}$ denote the mean vertical convective and turbulent mass fluxes, respectively, across the street canyon's top boundary ($z/H = 1$), through the exchange surface A (m^2). The denominator $[C]$ represents the spatially averaged pollutant concentration (g/m^3) inside the control volume. This volume encompasses the full extent of the street canyon, ranging from ground level up to either the rooftop height or pedestrian level.

- Personal intake fraction:
The personal intake fraction (P_{IF}) is defined as the proportion of pollutants inhaled by an individual relative to the total quantity of pollutants emitted. It is widely used in research focusing on human exposure to air pollutants in residential contexts.[4–6,20] In the present work, P_{IF} is applied to evaluate residents' exposure to traffic-related emissions within the target zone. The P_{IF} is determined as

$$P_{IF} = \frac{\sum_i^N (Br_i \times \Delta t_i \times Ce_i)}{M}, \tag{11}$$

where the subscript i denotes a specific type of residential environment where residents conduct daily activities. N denotes the overall set of environments under consideration. The term Br denotes the average individual breathing rate (m^3/s). Δt specifies the residence time (s). Ce indicates the spatially averaged concentration level (mg/m^3) obtained through LES simulations. M represents the total vehicular emission (kg). The computed P_{IF}, expressed in parts per million (ppm), signifies that an individual inhales 1 mg of pollutants per 1 kg emitted.

The indoor P_{IF} is calculated using the values of Ce, Δt, and Br for time spent at home ($N = 1$). Since the LES simulations only provide traffic-related pollutant concentrations for outdoor environments, indoor pollutant concentrations are inferred by assuming that outdoor air quality influences indoor conditions through natural and/or mechanical ventilation, which exchanges indoor air with outdoor air. Previous studies[63,64] have shown that indoor concentrations of pollutants originating from outdoor sources are generally comparable to those measured adjacent to building façades. On this basis, the indoor Ce is approximated from the façade-averaged mean CO concentration at the corresponding height.

This study focuses on the building-level average P_{IF} for occupants, without addressing intra-building variations in pollutant exposure across different indoor spaces. The indoor P_{IF} is evaluated for three age categories: young, adult, and elderly in this study. The data in Table V provide the breathing rates (Br_i) and time patterns [used to calculate indoor stay durations (Δt_i)] for different age groups, which vary according to their specific home activity patterns.

III. COMPARISON BETWEEN QUASI-2D AND 3D CONFIGURATION RESULTS

A. Mean wind velocity and mean concentration field

Figure 4 illustrates the flow patterns in a street canyon with a viaduct and 4-m-high bilateral noise barrier configuration. In the quasi-2D model [see Fig. 4(a)], two distinct flow features are observed: the large vertically rotating canyon vortices [recirculating along the canyon's longitudinal axis (y axis)] in the whole canyon, and small vertically rotating vortices between the two noise barriers on the viaduct. These phenomena are predominantly induced by the shear forces resulting from the skimming flow above the rooftops. These flow features in the quasi-2D model are also observed in the 3D model. However, the 3D model [as shown in Fig. 4(b)] exhibits more complex flow structures due to air entering the canyon laterally through building gaps and from the roof. In this case, 3D helical flows develop in the canyon, and channeling flows occur along the street aligned with the inflow wind direction. This flow pattern leads to the pollutant removal process contrasts with that in quasi-2D street canyons, where pollutant removal occurs primarily through vertical transport above the rooftop. In addition, horizontally rotating corner eddies [recirculating along the vertical axis (z axis)] are also observed in the 3D case [Fig. 4(d)]. These corner vortices are induced by shear at the street ends, generated by the channeling flow.

As the viaducts in the studied canyons are perpendicular to the approaching wind, the streamwise and vertical velocity components are more significantly affected. Therefore, vector fields at streamwise slices (i.e., x–z planes in quasi-2D and 3D models) are plotted in Fig. 5, which provides a clearer view of how flow patterns vary due to viaduct configurations. In the quasi-2D models [see Fig. 5(a)], the no-viaduct case (NV_{2d}) shows a main clockwise vortex, with the vortex center located near the middle of the canyon. When a viaduct is introduced ($Vb0_{2d}$), the main clockwise vortex persists, but its center shifts slightly upward, positioned above the viaduct. When noise barriers are installed on the viaduct (cases $Vb2_{2d}$ and $Vb4_{2d}$), the main clockwise

TABLE V. Daily breathing rates and time patterns for different age groups in home indoor environments (data from Refs. 57 and 60).

Age group	Young group (ages 6–18)	Adults group (ages 18–60)	Elderly group (aged above 60)
Daily breathing rates (m^3/day)	12.5	13.8	13.1
Time patterns (%)	60.1	58.1	70.2

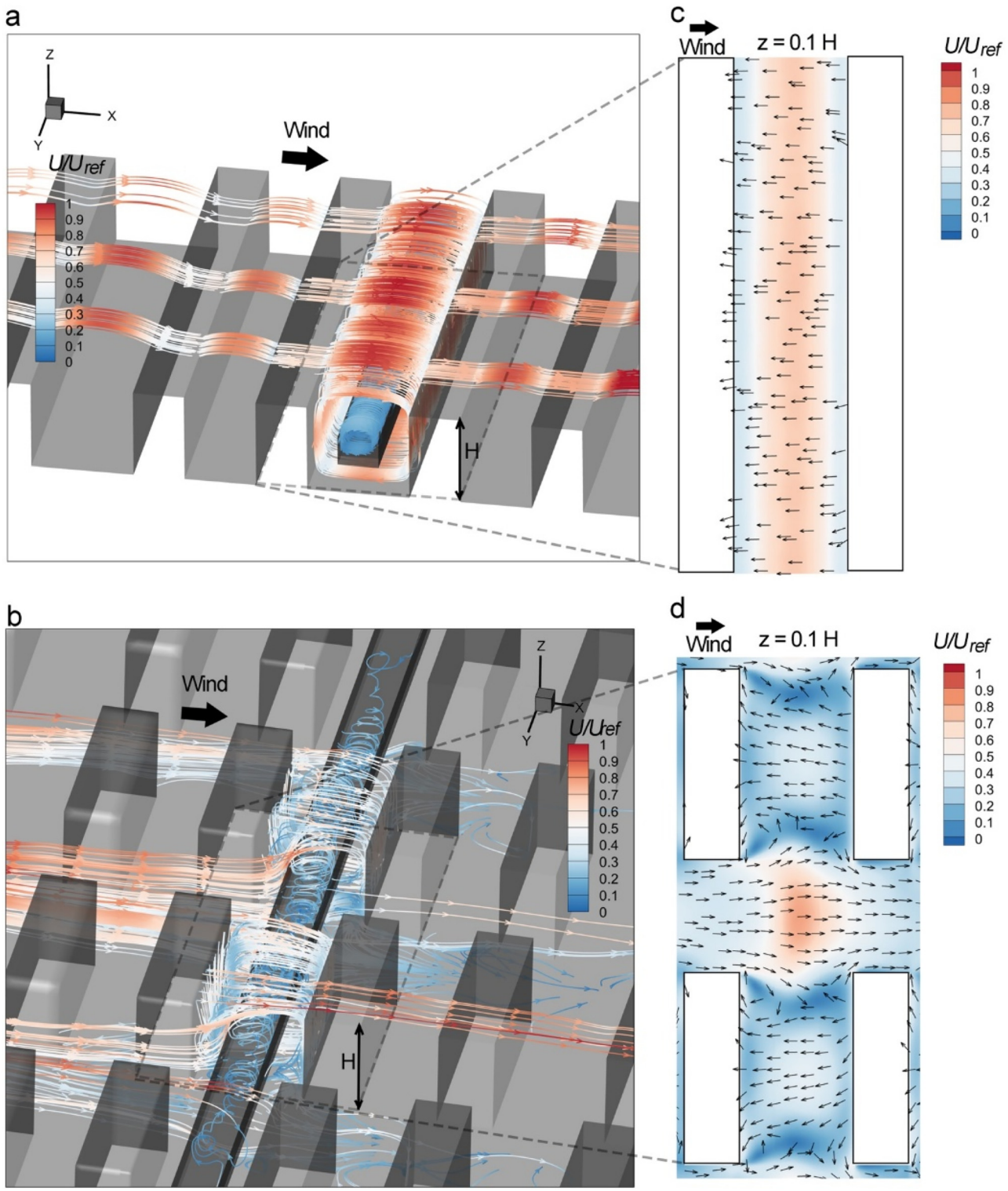

FIG. 4. Flow patterns in a regular street canyon with a viaduct and 4-m-high noise barriers: 3D streamlines of mean wind velocity in the (a) quasi-2D model and (b) 3D model; vector field of mean wind velocity at horizontal plane (at $z/H = 0.1$) in the (c) quasi-2D model and (d) 3D model.

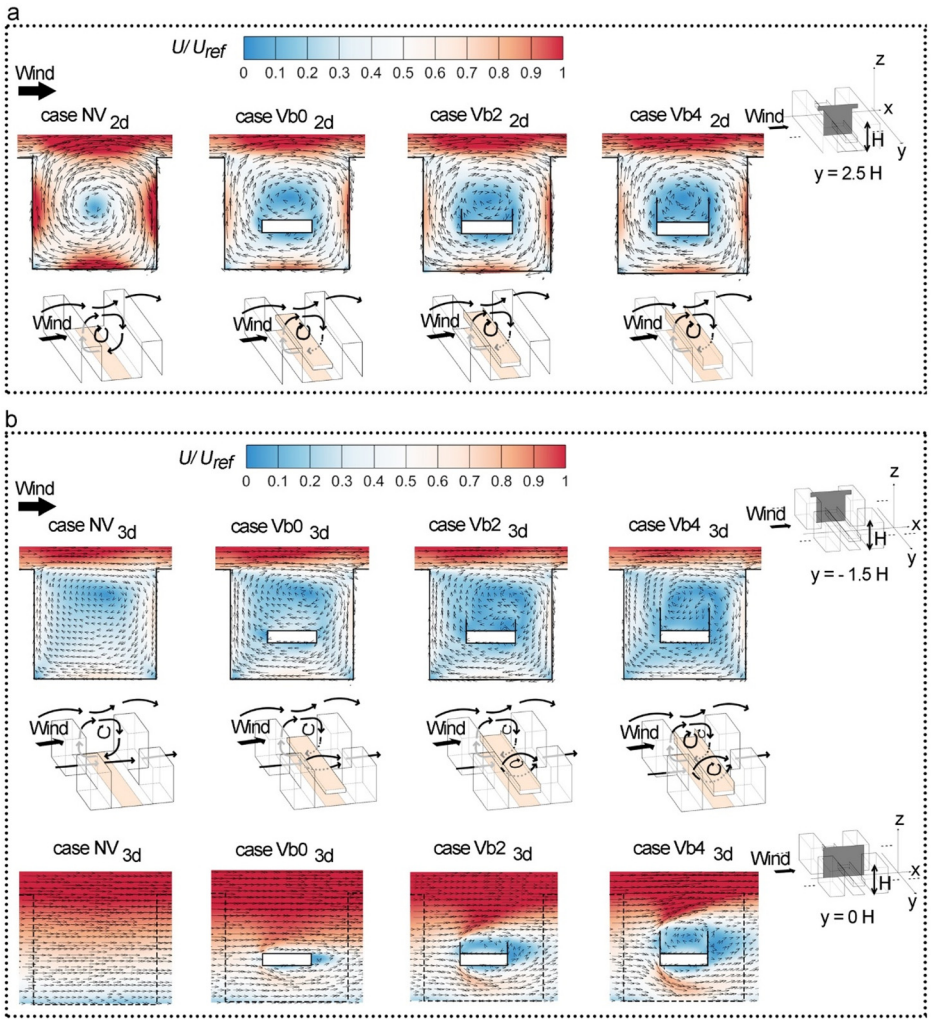

FIG. 5. Vector field and dimensionless mean wind velocity (U/U_{ref}) in the street canyon's streamwise cross sections (x–z planes): (a) quasi-2D model at the middle cross section ($y = 2.5H$); (b) 3D model at the middle cross section ($y = -1.5H$) and at the building-gap cross section ($y = 0H$).

vortex remains, and the vortex center is located similarly to the case without noise barriers.

In the 3D models [see Fig. 5(b)], the no-viaduct case (NV_{3d}) also exhibits a main clockwise vortex in the middle cross section, but its center is located near the roof level of the canyon. This upward shift of the main vortex compared to the quasi-2D case is attributed to lateral inflow. This finding supports previous studies showing that street length can significantly affect the flow regime, even with the same aspect ratio. When a viaduct is introduced ($Vb0_{3d}$), the main clockwise vortex remains in the middle cross section. Its center is slightly elevated above the viaduct, consistent with the quasi-2D case. However, when noise barriers are added on the viaduct (cases $Vb2_{3d}$ and $Vb4_{3d}$), the main vortex structure in both the middle ($y = -1.5H$) and building-gap cross sections ($y = 0H$) is disrupted. In addition, a smaller clockwise vortex forms near the windward-side barrier. This result contrasts significantly with the quasi-2D cases.

Figure 6 presents the mean pollutant concentration fields at streamwise slices of street canyons for the four studied cases, obtained from quasi-2D and 3D models. In the quasi-2D models, case NV_{2d} shows pollutant retention along the leeward wall, driven by the dominant clockwise vortex [see Fig. 6(a)]. When a viaduct is introduced ($Vb0_{2d}$), the high-concentration region shifts upward toward the viaduct level. With the addition of noise barriers on the viaduct (cases $Vb2_{2d}$ and $Vb4_{2d}$), this high-concentration region remains around the viaduct zone. As the barrier height increases, pollutant accumulation becomes more pronounced, particularly along the leeward-side barrier.

The pollutant dispersion patterns in the cross section at $y = -1.5H$ of the 3D models shown in Fig. 6(b) across the four studied cases closely resemble those in the middle cross section at $y = 2.5H$ of the quasi-2D models as shown in Fig. 6(a). However, the pollutant concentrations at corresponding locations are significantly lower in the 3D cases compared to the quasi-2D cases. This is primarily because pollutant removal in 3D models occurs through both lateral dispersion via building gaps [as shown in the cross section at $y = 0H$ in Fig. 6(b)] and vertical escape through the roof level. In contrast, in quasi-2D models, pollutant removal is limited solely to vertical escape through the roof level. This suggests that quasi-2D models of street canyons

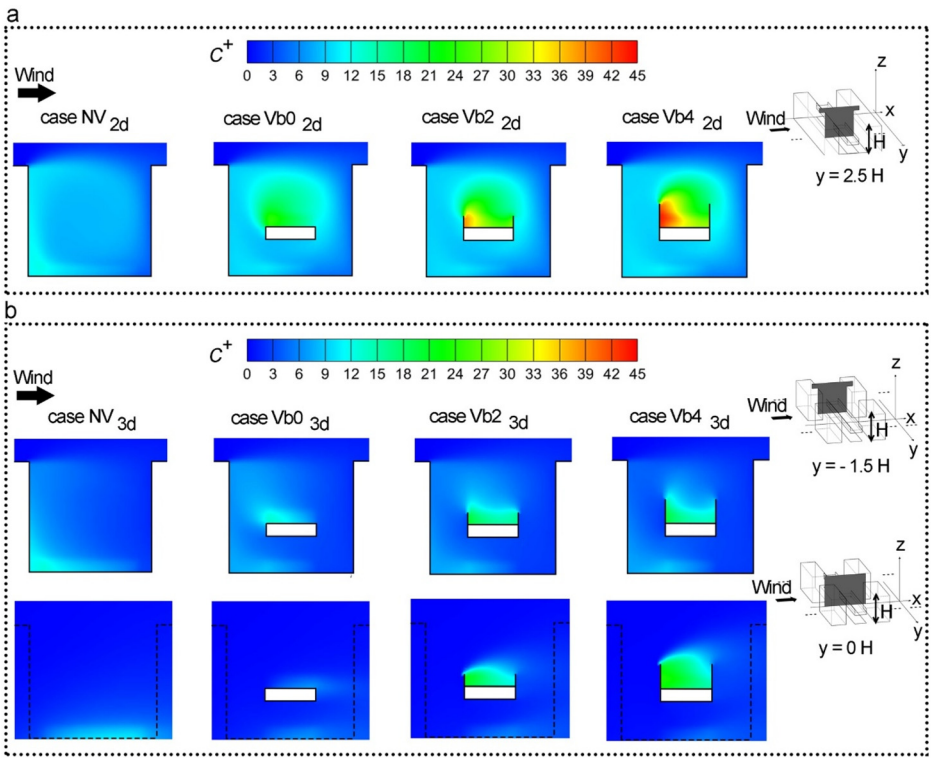

FIG. 6. Dimensionless mean pollutant concentration (C^+) in the street canyon's streamwise cross sections (x–z planes): (a) quasi-2D model at the middle cross section ($y = 2.5H$); (b) 3D model at the middle cross section ($y = -1.5H$) and at the building-gap cross section ($y = 0H$).

with viaducts tend to overestimate pollutant concentrations compared to more realistic 3D configurations.

To compare the overall pollution concentrations in the quasi-2D and 3D street canyons, we evaluate the spatially averaged pollutant concentration ([C]) in both quasi-2D and 3D models. As shown in Fig. 7(a), the values of [C] for the entire canyon (zone height: 18 m from ground level) are more than twice as high in the quasi-2D cases as those in the 3D cases. However, the variation in [C] across the three viaduct configurations shows a similar increasing trend in both quasi-2D and 3D models. For the pedestrian-level zone (zone height: 2 m from ground level), the values of [C] in the quasi-2D cases are higher than those in the 3D cases, with absolute differences in [C] ranging from 0.03 to 0.49 mg/m^3—up to 1.8 times greater than in the 3D cases [see Fig. 7(b)]. Additionally, for the 3D models, the values of [C] for the pedestrian-level zone in the cases NV, Vb0, Vb2, and Vb4 decrease sequentially. In contrast, the quasi-2D models show minimal variation in [C] across these cases. This indicates that, while the quasi-2D models may capture the general trend of pollutant concentration in the whole canyon, they fail to accurately represent pedestrian-level pollutant concentration variations across different viaduct configurations.

Additionally, we further evaluate the area-averaged pollutant concentration (C_{avg}) along the building facades at every floor level for both the quasi-2D [see Figs. 8(a)–8(d)] and 3D [see Figs. 8(e)–8(h)] models. In the quasi-2D models, three buildings are considered, labeled L4 to L6. These correspond to buildings in the 3D model as follows: L4 to B7 and B8, L5 to B9 and B10, and L6 to B11 and B12. For these studied buildings in the target zone, each with a façade height of 18 m, the height is divided into six levels: 0–3 m for the first level, 3–6 m for the second, and so on in 3 m increments. C_{avg} at each level is calculated using data from all façades of each building, representing indoor air quality. Note that C_{avg} on four facades in 3D models and C_{avg} on two facades in quasi-2D models were used to calculate the C_{avg} at each building level, as illustrated in Fig. 8.

Across all four studied cases in both quasi-2D and 3D models, a consistent trend is observed: buildings located on the leeward-side street canyon (L4 in quasi-2D models or B7 and B8 in 3D models) exhibit the highest C_{avg}. The buildings away from the road within the residential area (L6 in quasi-2D models or B11 and B12 in 3D models) show the lowest C_{avg}. Meanwhile, the variations of C_{avg} along the building height are also different in the quasi-2D and 3D models. In the quasi-2D models, the values of C_{avg} remain nearly constant from level 1 to level 6 for both L4 and L6, indicating little vertical variation in pollutant concentration. In contrast, the 3D models show a significant decrease in C_{avg} with increasing height, particularly for buildings B7/B8 and B9/B10.

Moreover, in the 3D models, the maximum C_{avg} values decrease sequentially from case NV (1.12 mg/m^3) to cases Vb0, Vb2, and Vb4, which are reduced by 0.41, 0.45, and 0.47 mg/m^3, respectively, relative to case NV. In contrast, the quasi-2D models do not exhibit this trend, with maximum C_{avg} values for cases NV, Vb0, Vb2, and Vb4 being 0.81, 0.66, 0.67, and 0.68 mg/m^3, respectively. This indicates the inadequacy of the quasi-2D models in accurately capturing the variations in area-averaged pollutant concentrations across different viaduct configurations.

B. Mean mass fluxes and mean pollutant exchange velocity

Figure 9 presents the $Q_{c,z}/Q_0$ and $Q_{t,z}/Q_0$ of inflow and outflow mass fluxes at the canyon roof level ($z/H = 1$). Positive values correspond

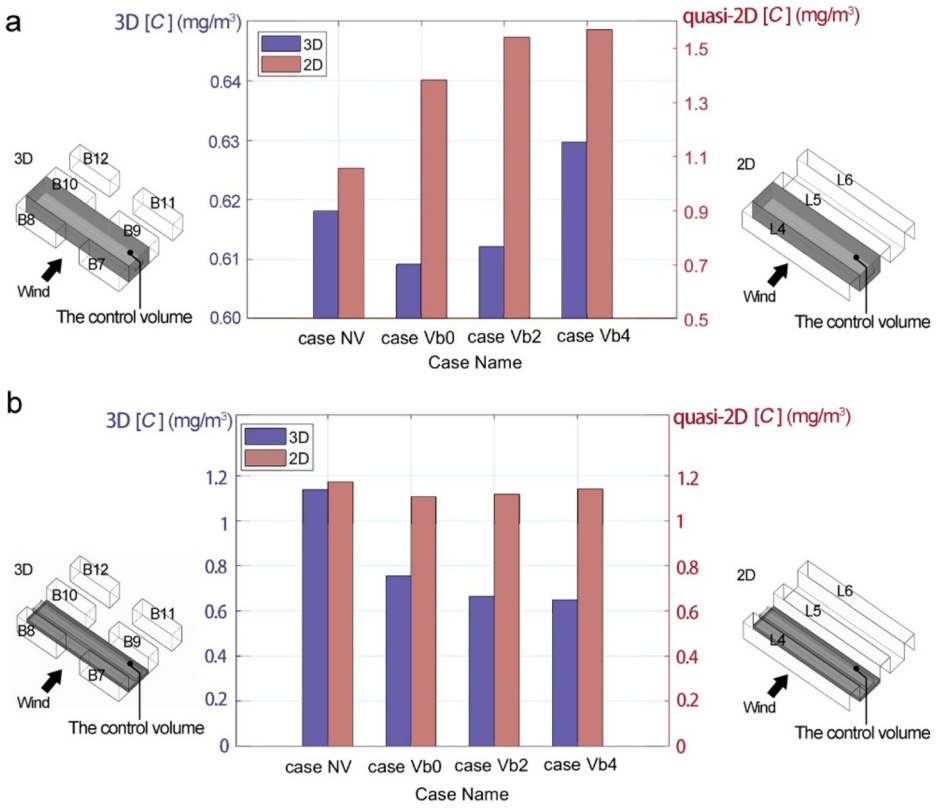

FIG. 7. Spatially averaged pollutant concentration [*C*] inside the control volume in quasi-2D and 3D models: (a) in the entire canyon (volume height: 18 m from ground level) and (b) in the pedestrian-level zone (volume height: 2 m from ground level).

to outflow mass fluxes, whereas negative values represent inflow mass fluxes, with the latter shown in absolute form for clarity. Overall, both inflow and outflow mass fluxes are significantly higher in the quasi-2D models than in the 3D models across all four studied cases. For the inflow mass fluxes, the quasi-2D models [see Fig. 9(a)] are dominated by the convective component ($Q_{c,z}/Q_0$) across all four studied cases, with values gradually decreasing from NV to Vb0, Vb2, and Vb4. In contrast, in the 3D models [see Fig. 9(b)], the inflow mass fluxes are primarily dominated by the turbulent component ($Q_{t,y}/Q_0$) and similarly show a decreasing trend across the same sequence of cases. For the outflow mass fluxes, the quasi-2D models [see Fig. 9(c)] remain dominated by the convective component ($Q_{c,z}/Q_0$), with its magnitude decreasing as the cases transition from NV to Vb0, Vb2, and Vb4. In the 3D models [see Fig. 9(d)], the outflow mass fluxes are also dominated by the convective component ($Q_{c,z}/Q_0$), with similar values observed across all four cases.

Figure 10 illustrates the area-averaged U_e/U_{ref} for both quasi-2D and 3D models. The U_e/U_{ref} is separated into two contributions: the convective component ($U_{e,c}/U_{ref}$) and the turbulent component ($U_{e,t}/U_{ref}$). In all four cases, the convective component dominates in both quasi-2D and 3D models. However, the values of $U_{e,c}/U_{ref}$ are generally higher in the 3D models than in the quasi-2D models, with absolute differences in $U_{e,c}/U_{ref}$ reaching up to 0.013 (corresponding to increases of 25.5%). In the quasi-2D models, $U_{e,c}/U_{ref}$ exhibits a decreasing trend from NV (0.075) to Vb0 (0.057), Vb2 (0.051), and Vb4 (0.050). In contrast, the 3D models display an opposite trend, where $U_{e,c}/U_{ref}$ in case NV (0.061) is lower than that in cases Vb0 (0.066), Vb2 (0.064), and Vb4 (0.062). For the values of U_e/U_{ref}, 3D models generally show higher values than in the quasi-2D models, with absolute differences in U_e/U_{ref} reaching up to 0.028 (in case Vb2)—an increase in up to 33.6% compared to the quasi-2D cases. This highlights the difference in roof-level pollutant removal effectiveness between the quasi-2D and 3D models.

C. Indoor personal intake fraction

Indoor pollutant exposure is primarily influenced by the duration of time spent indoors. Meanwhile, the pollutant spatial distribution is largely controlled by surrounding road configurations. As a result, the indoor P_{IF} patterns are similar across all three age groups under a given scenario. For the sake of conciseness, results specific to the elderly group are presented.

Figure 11 shows the indoor P_{IF} experienced by the elderly group across levels 1–6 of the selected buildings in the quasi-2D and 3D models. A consistent pattern emerges across all four studied cases in both the quasi-2D and 3D models: buildings situated on the leeward-side street canyon (L4 in the quasi-2D models or B7 and B8 in the 3D models) consistently experience the highest levels of indoor P_{IF}. The outermost buildings in the residential area near the road (L6 in the quasi-2D models or B11 and B12 in the 3D models) exhibit the lowest indoor P_{IF} values. Meanwhile, the vertical distribution of P_{IF} differs markedly between the quasi-2D and 3D models. In the quasi-2D models, indoor P_{IF} values for both L4 and L6 remain nearly uniform across levels 1–6, suggesting limited vertical variability in indoor P_{IF}. In

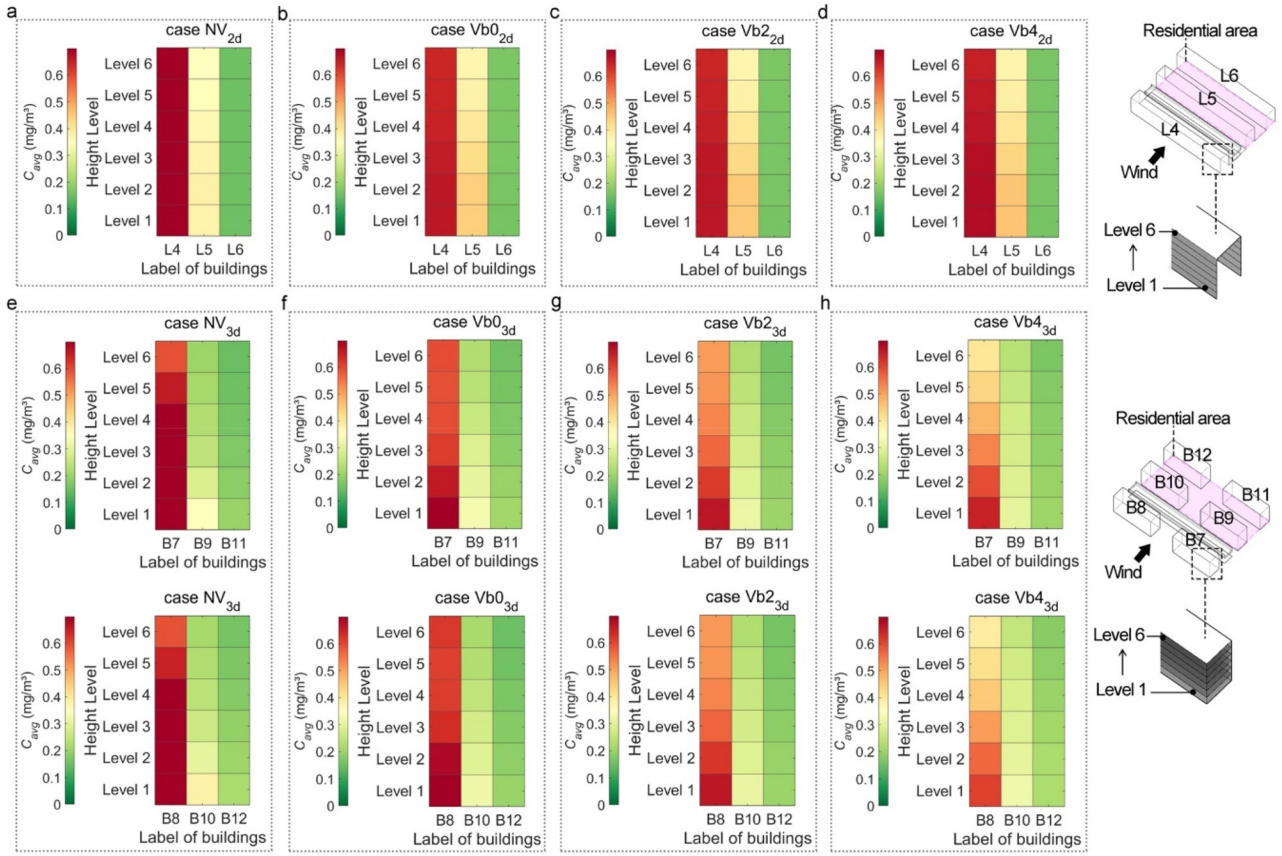

FIG. 8. Area-averaged pollutant concentration (C_{avg}) on building façades for each level in the (a)–(d) quasi-2D models and (e)–(h) 3D models.

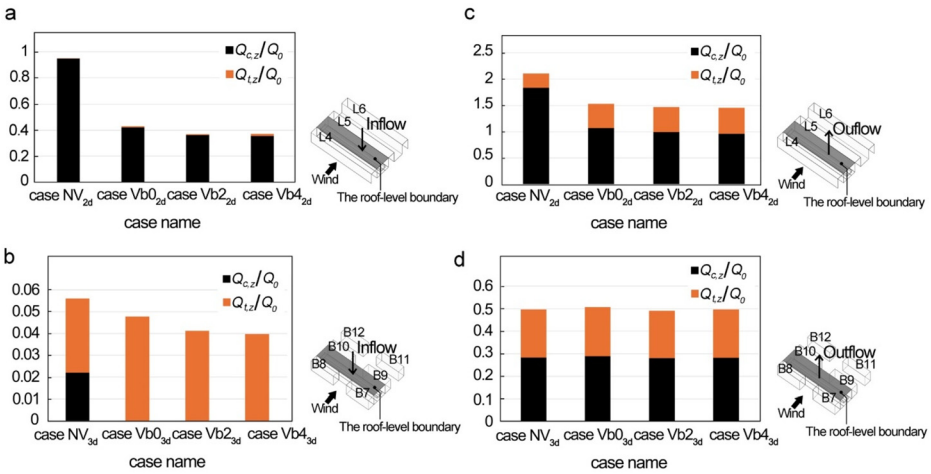

FIG. 9. Roof-level ($z/H = 1$) area-averaged $Q_{c,z}/Q_0$ and $Q_{t,z}/Q_0$ for inflow [(a) and (b)] and outflow [(c) and (d)] in the target zone, comparing studied cases of quasi-2D models [(a) and (c)] and 3D [(b) and (d)] models.

contrast, the 3D models reveal a significant decrease in indoor P_{IF} with increasing height, particularly in buildings B7/B8 and B9/B10. These findings emphasize the inability of quasi-2D models to adequately capture vertical gradients in indoor pollutant exposure.

Moreover, in the 3D models, the maximum indoor P_{IF} values decrease significantly from the no-viaduct case (NV_{3d}) (0.233 ppm) to the viaduct without noise barriers case ($Vb0_{3d}$) (0.150 ppm). When noise barriers are introduced [$Vb2_{3d}$ (0.137 ppm) and $Vb4_{3d}$

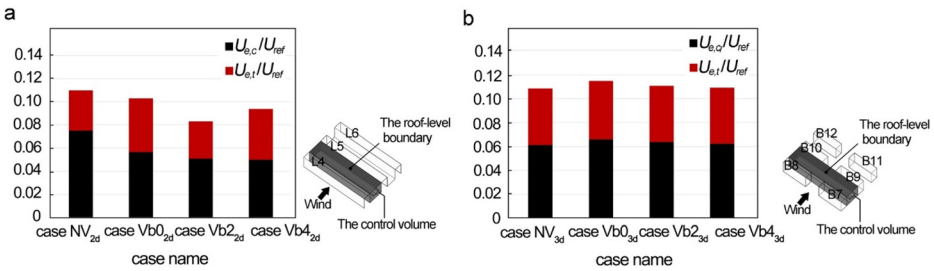

FIG. 10. Roof-level ($z/H = 1$) area-averaged U_e/U_{ref} in the target zone in (a) quasi-2D models and (b) 3D models.

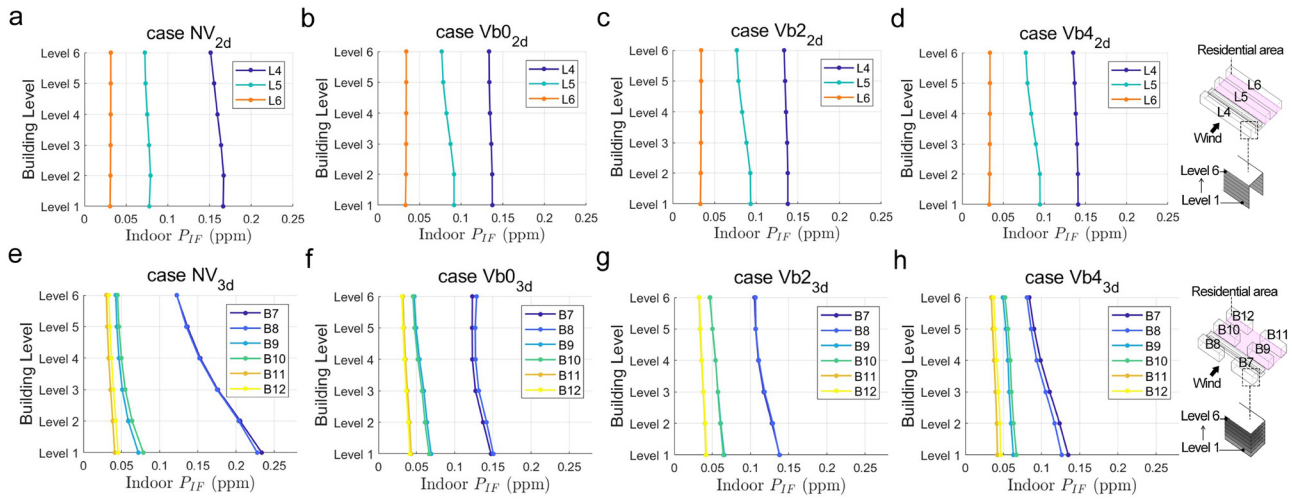

FIG. 11. Indoor P_{IF} of the elderly group from building levels 1–6 for the four cases in (a)–(d) quasi-2D models and (e)–(h) 3D models.

(0.134 ppm)], the maximum indoor P_{IF} values further decrease compared to $Vb0_{3d}$. However, an increase in the noise barrier height from $Vb2_{3d}$ to $Vb4_{3d}$ does not produce a further reduction in the maximum indoor P_{IF}. In contrast, the quasi-2D models show a decrease in the maximum indoor P_{IF} values from NV_{2d} (0.167 ppm) to $Vb0_{2d}$ (0.137 ppm), but the adoption of noise barriers [$Vb2_{2d}$ (0.138 ppm) and $Vb4_{2d}$ (0.141 ppm)] does not lead to any further decrease in the maximum indoor P_{IF} values.

For the mean indoor P_{IF} evaluated over the six levels of the studied building, several observations can be made: (1) For leeward-side buildings in the canyon (L4 in quasi-2D models or B7/B8 in 3D models), the mean indoor P_{IF} is similar between the quasi-2D and 3D models in cases NV and Vb0. However, in cases Vb2 and Vb4, the quasi-2D models show higher mean indoor P_{IF} values than those in 3D models by approximately 0.02 and 0.04 ppm, corresponding to increases of 16.7% and 36.5%, respectively. (2) For windward-side buildings in the canyon (L5 in quasi-2D models and B9/B10 in 3D models), the mean indoor P_{IF} is higher in the quasi-2D models than in the 3D models across all four studied cases, with the maximum difference reaching up to 0.03 ppm (in case Vb4), corresponding to increases of 54.79%. (3) For outermost buildings in the residential area near the road (L6 in quasi-2D models or B11/B12 in 3D models), the mean indoor P_{IF} is similar between the quasi-2D and 3D models across all four studied cases. These observations indicate that quasi-2D models can reasonably represent the mean indoor pollutant exposure in buildings away from the road. However, they cannot accurately capture the mean indoor pollutant exposure in near-road buildings, especially under viaduct configurations with noise barriers.

IV. DISCUSSION

This study reveals key differences between LES simulations using quasi-2D and 3D street canyon models. With the current settings, quasi-2D models fail to capture horizontally rotating corner eddies caused by lateral flows through building gaps—features that are clearly present in 3D models. This finding is consistent with previous RANS studies (e.g., Ref. 34). Moreover, the quasi-2D models are inadequate to reproduce the disruption of the mean wind flow structure induced by noise barriers occurs in 3D models, a finding not previously highlighted in the literature. These flow pattern differences lead to distinct pollutant dispersion patterns between quasi-2D and 3D models. In quasi-2D models, wind flow cannot penetrate through side gaps, whereas in 3D models, lateral flows enhance pollutant transport and removal. As a result, LES simulations with quasi-2D street canyon models generally yield higher estimates of both pollutant concentrations and indoor P_{IF} compared to 3D models. More importantly, this study shows that the inadequacy of quasi-2D models in capturing the vertical gradient of area-averaged pollutant concentrations on building façades and indoor P_{IF}, which is clearly captured in 3D models across all tested cases. To the best of our knowledge, this difference between

quasi-2D and 3D models has not been explicitly identified in previous studies.

Several limitations of this study should be acknowledged:

The analysis focused on a typical street canyon configuration, without considering deeper or height-asymmetrical street canyons, as well as the effects of urban green infrastructure. Future research could explore a wider range of aspect ratios, building geometries, viaduct heights, noise barrier types, and incorporate urban greenery. By examining a broader set of cases, it may become possible to identify specific scenarios in which 3D street canyon models can be effectively replaced by quasi-2D models.

This study was conducted under isothermal conditions. In real urban environments, however, low ambient wind speeds combined with heat released from building surfaces can significantly influence pollutant dispersion. Future work should account for the combined influence of wind and buoyancy or under stratified boundary layer flows.[65]

V. CONCLUSION

This study investigated the differences between quasi-2D and 3D models for LES simulation of traffic pollutant dispersion in street canyons with urban viaduct configurations. Four representative cases were examined within a regular street canyon under perpendicular wind conditions, including ground-level roads only, viaducts without noise barriers, and viaducts with bilateral noise barriers of 2 or 4 m in height. The analysis focused on five key parameters: mean wind velocity, mean pollutant concentration fields, mean vertical mass fluxes, pollutant exchange velocity, and personal intake fraction (P_{IF}) to evaluate pollutant dispersion within the canyon.

The results demonstrate that these models yield fundamentally different pollutant transport mechanisms, and the differences are exaggerated in the viaduct configurations with noise barriers. The major conclusions are given as follows:

- Regarding the wind flow field, the main difference of wind flow patterns between the quasi-2D and 3D models is the presence of horizontally rotating corner eddies, which arise due to lateral flows through building gaps in the 3D cases. In addition, the quasi-2D models cannot reproduce the disrupted mean wind flow structure caused by the installation of noise barriers, which is clearly observed in the 3D models.
- Regarding the pollutant dispersion field, at the streamwise slices with buildings, the pollutant dispersion patterns in the quasi-2D models show a similar trend to those in the 3D models across all four studied scenarios. However, pollutant concentrations at corresponding locations are significantly lower in the 3D cases than in the quasi-2D cases. The comparison also shows the inadequacy of quasi-2D models in reproducing the pollutant concentration variations at the pedestrian-level zones or building facades for different viaduct configurations.
- Regarding the indoor pollutant exposure, the quasi-2D models predict similar values for buildings away from the road compared with 3D models. However, they fail to accurately capture exposure levels in near-road buildings under viaduct configurations, especially those with noise barriers, as observed in simulations with a 3D model. Compared to the 3D models, quasi-2D models generally overestimate the mean indoor personal intake fraction (P_{IF}) across the six building levels. In both quasi-2D and 3D models across all four cases, the convective component of outflow mean vertical mass fluxes dominates pollutant removal. The dimensionless convective pollutant exchange velocity ($U_{e,c}/U_{ref}$) consistently exhibits higher values in the 3D models, indicating that roof-level pollutant removal is more efficient in the 3D models than in quasi-2D ones.

Overall, when applying CFD simulation results using quasi-2D street canyon models in urban design practice, it is essential to consider the appropriate application scenarios. For evaluating overall air quality within the entire street canyon or assessing traffic-related pollutant exposure experienced by occupants of buildings situated away from the road, quasi-2D models may provide acceptable approximations. However, for assessing pedestrian-level air quality or evaluating pollutant exposure experienced by occupants of buildings situated close to the road, quasi-2D street canyon models are not suitable due to their inability to accurately capture near-road dispersion dynamics and vertical pollutant gradients, especially in the viaduct configurations with noise barriers.

SUPPLEMENTARY MATERIAL

See the supplementary material for S1: CFD Validation for Pollutant Dispersion in Street Canyons.

ACKNOWLEDGMENTS

We acknowledge the support of a grant from City University of Hong Kong (Project No. 9610684) and a grant from the Hong Kong Environment and Conservation Fund (Project No. 74/2022), as well as HPC resources provided by Beijing PARATERA Tech Co., Ltd., which contributed to the results reported in this paper. Additionally, we acknowledge the contributions of Mr. Sihan Wen for his assistance with the CFD modeling.

AUTHOR DECLARATIONS

Conflict of Interest

The authors have no conflicts to disclose.

Author Contributions

Lemei Li: Conceptualization (equal); Formal analysis (equal); Investigation (equal); Visualization (equal); Writing – original draft (equal); Writing – review & editing (equal). **Bin Lu:** Writing – review & editing (equal). **Peng Qin:** Writing – review & editing (equal). **Lili Xia:** Writing – review & editing (equal). **Jun Cai:** Project administration (equal). **Jing Dong:** Writing – review & editing (equal). **Pengyuan Shen:** Writing – review & editing (equal). **Huanhuan Wang:** Writing – review & editing (equal). **Zhen Han:** Writing – review & editing (equal). **Guangdong Duan:** Writing – review & editing (equal). **Dengkai Chi:** Writing – review & editing (equal). **Yunfei Fu:** Writing – review & editing (equal). **Qiusheng Li:** Project administration (equal). **Xing Zheng:** Conceptualization (equal); Funding acquisition (equal); Investigation (equal); Methodology (equal); Software (equal); Supervision (equal); Validation (equal); Writing – original draft (equal); Writing – review & editing (equal).

DATA AVAILABILITY

The data that support the findings of this study are available from the corresponding author upon reasonable request.

REFERENCES

[1]Y. Liu, K. Han, and Z. Yang, "Impact of traffic policy on travel population exposure during heavy pollution episodes: A Chengdu case study," Urban Clim. **55**, 101886 (2024).

[2]X. Zheng and J. Yang, "Urban road network design for alleviating residential exposure to traffic pollutants: Super-block or Mini-block?" Sustainable Cities Soc. **89**, 104327 (2023).

[3]N. de Oliveira Gurjão, J. L. Oliveira Lucas Júnior, L. Sucupira Furtado, and J. B. Soares, "Air pollution dynamics in Fortaleza, Brazil: Exploring the interplay of traffic and high-rise development," Urban Clim. **58**, 102176 (2024).

[4]K. Zhang, G. Chen, X. Wang, S. Liu, C. M. Mak, Y. Fan, and J. Hang, "Numerical evaluations of urban design technique to reduce vehicular personal intake fraction in deep street canyons," Sci. Total Environ. **653**, 968–994 (2019).

[5]J. Hang, Z. Luo, X. Wang, L. He, B. Wang, and W. Zhu, "The influence of street layouts and viaduct settings on daily carbon monoxide exposure and intake fraction in idealized urban canyons," Environ. Pollut. **220**, 72–86 (2017).

[6]L. He, J. Hang, X. Wang, B. Lin, X. Li, and G. Lan, "Numerical investigations of flow and passive pollutant exposure in high-rise deep street canyons with various street aspect ratios and viaduct settings," Sci. Total Environ. **584–585**, 189–206 (2017).

[7]J. Hang, M. Lin, D. C. Wong, X. Wang, B. Wang, and R. Buccolieri, "On the influence of viaduct and ground heating on pollutant dispersion in 2D street canyons and toward single-sided ventilated buildings," Atmos. Pollut. Res. **7**, 817–832 (2016).

[8]C. Lin, R. Ooka, H. Kikumoto, C. Flageul, Y. Kim, Y. Zhang, and K. Sartelet, "Impact of solid road barriers on reactive pollutant dispersion in an idealized urban canyon: A large-eddy simulation coupled with chemistry," Urban Clim. **55**, 101989 (2024).

[9]P. Qin, A. Ricci, and B. Blocken, "CFD simulation of pollutant dispersion in a street canyon with realistic car sources: The potential of green infrastructure configurations," Urban Clim. **62**, 102544 (2025).

[10]Z. Li, T. Ming, T. Shi, H. Zhang, C.-Y. Wen, Y. Wu, C. Wang, K. Yin, R. de Richter, and W. Li, "CFD modeling of traffic tidal flow: Assessment of pollutant dispersion," Urban Clim. **47**, 101380 (2023).

[11]P. Ghobadi and N. Nasrollahi, "Assessment of pollutant dispersion in deep street canyons under different source positions: Numerical simulation," Urban Clim. **40**, 101027 (2021).

[12]J. Li, W. You, Y. Peng, and W. Ding, "Exploring the potential of the aspect ratio to predict flow patterns in actual urban spaces for ventilation design by comparing the idealized and actual canyons," Sustainable Cities Soc. **102**, 105214 (2024).

[13]S. Vardoulakis, B. E. A. Fisher, K. Pericleous, and N. Gonzalez-Flesca, "Modelling air quality in street canyons: A review," Atmos. Environ. **37**, 155–182 (2003).

[14]K.-F. Lu and Z.-R. Peng, "Impacts of viaduct and geometry configurations on the distribution of traffic-related particulate matter in urban street canyon," Sci. Total Environ. **858**, 159902 (2023).

[15]T. Ming, F. He, Y. Wu, T. Shi, C. Su, C. Wang, Z. Li, W. Chen, and R. De Richter, "The effect of noise barriers on viaducts on pollutant dispersion in complex street canyons," Energy Built Environ. **4**, 589–600 (2023).

[16]C. Hao, X. Xie, Y. Huang, and Z. Huang, "Study on influence of viaduct and noise barriers on the particulate matter dispersion in street canyons by CFD modeling," Atmos. Pollut. Res. **10**, 1723–1735 (2019).

[17]J. Hang, R. Buccolieri, X. Yang, H. Yang, F. Quarta, and B. Wang, "Impact of indoor-outdoor temperature differences on dispersion of gaseous pollutant and particles in idealized street canyons with and without viaduct settings," Build. Simul. **12**, 285–297 (2019).

[18]X. Zheng and J. Yang, "Impact of moving traffic on pollutant transport in street canyons under perpendicular winds: A CFD analysis using large-eddy simulations," Sustainable Cities Soc. **82**, 103911 (2022).

[19]Z. T. Ai and C. M. Mak, "CFD simulation of flow in a long street canyon under a perpendicular wind direction: Evaluation of three computational settings," Build. Environ. **114**, 293–306 (2017).

[20]J. Hang, Z. Xian, D. Wang, C. M. Mak, B. Wang, and Y. Fan, "The impacts of viaduct settings and street aspect ratios on personal intake fraction in three-dimensional urban-like geometries," Build. Environ. **143**, 138–162 (2018).

[21]T. Ming, C. Nie, W. Li, X. Kang, Y. Wu, M. Zhang, and C. Peng, "Numerical study of reactive pollutants diffusion in urban street canyons with a viaduct," Build. Simul. **15**, 1227–1241 (2022).

[22]H. Zhi, Z. Qiu, W. Wang, G. Wang, Y. Hao, and Y. Liu, "The influence of a viaduct on PM dispersion in a typical street: Field experiment and numerical simulations," Atmos. Pollut. Res. **11**, 815–824 (2020).

[23]A. Issakhov, P. Omarova, and A. Abylkassymova, "Determination of optimal height of barriers to reduce the amount of pollution in the viaduct settings in an idealized urban canyon: A numerical study," Environ. Monit. Assess. **195**, 178 (2023).

[24]C. Zhang, M. Wen, J. Zeng, G. Zhang, H. Fang, and Y. Li, "Modeling the impact of the viaduct on particles dispersion from vehicle exhaust in street canyons," Sci. China Technol. Sci. **55**, 48–55 (2012).

[25]D.-N. Lu, H.-D. He, Z. Wang, H.-M. Zhao, and Z.-R. Peng, "Impact of urban viaducts on the vertical distribution of fine particles in street canyons," Atmos. Pollut. Res. **14**, 101726 (2023).

[26]S. Ding, Y. Huang, P. Cui, J. Wu, M. Li, and D. Liu, "Impact of viaduct on flow reversion and pollutant dispersion in 2D urban street canyon with different roof shapes - Numerical simulation and wind tunnel experiment," Sci. Total Environ. **671**, 976–991 (2019).

[27]Y. Huang and Z. Zhou, "A numerical study of airflow and pollutant dispersion inside an urban street canyon containing an elevated expressway," Environ. Model. Assess. **18**, 105–114 (2013).

[28]R. Xu, T. Chen, Y. X. Fu, J. C. Chen, and Y. H. Liu, "Simulation study on impacts of viaduct height on pollutant dispersion in street canyons using LES and RANS models," J. Appl. Fluid Mech. **17**, 2775–2790 (2024).

[29]L. Chen, C. M. Mak, J. Hang, Y. Dai, J. Niu, and K. T. Tse, "Large eddy simulation study on pedestrian-level wind environments around elevated walkways and influential factors in ideal urban street canyons," Build. Environ. **235**, 110236 (2023).

[30]G. Duan, P. Brimblecombe, Y. L. Chu, and K. Ngan, "Turbulent flow and dispersion inside and around elevated walkways," Build. Environ. **173**, 106711 (2020).

[31]T. L. Chan, G. Dong, C. W. Leung, C. S. Cheung, and W. T. Hung, "Validation of a two-dimensional pollutant dispersion model in an isolated street canyon," Atmos. Environ. **36**, 861–872 (2002).

[32]T. R. Oke, "Street design and urban canopy layer climate," Energy Build. **11**, 103–113 (1988).

[33]T. Michioka, H. Takimoto, and A. Sato, "Large-eddy simulation of pollutant removal from a three-dimensional street canyon," Bound.-Layer Meteorol. **150**, 259–275 (2014).

[34]S.-J. Mei, Z. Luo, F.-Y. Zhao, and H.-Q. Wang, "Street canyon ventilation and airborne pollutant dispersion: 2-D versus 3-D CFD simulations," Sustainable Cities Soc. **50**, 101700 (2019).

[35]A. Afshari and N. Ramirez, "Improving the accuracy of simplified urban canopy models for arid regions using site-specific prior information," Urban Clim. **35**, 100722 (2021).

[36]X. Zheng and J. Yang, "CFD simulations of wind flow and pollutant dispersion in a street canyon with traffic flow: Comparison between RANS and LES," Sustainable Cities Soc. **75**, 103307 (2021).

[37]A. Rakai and J. Franke, "Validation of two RANS solvers with flow data of the flat roof Michelstadt case," Urban Clim. **10**, 758–768 (2014).

[38]X. Zheng, H. Montazeri, and B. Blocken, "CFD analysis of the impact of geometrical characteristics of building balconies on near-façade wind flow and surface pressure," Build. Environ. **200**, 107904 (2021).

[39]A. Niroobakhsh, S. Hassanzadeh, and F. Hosseinibalam, "The vital importance of dispersive fluxes on turbulent flow and pollution ventilation in street canyons," Urban Clim. **41**, 101032 (2022).

[40]B. Blocken, "LES over RANS in building simulation for outdoor and indoor applications: A foregone conclusion?" Build. Simul. **11**, 821–870 (2018).

[41]C. Gromke and B. Ruck, "On the impact of trees on dispersion processes of traffic emissions in street canyons," Boundary Layer Meteorol. **131**, 19–34 (2009).

[42]C. Gromke and B. Ruck, "Influence of trees on the dispersion of pollutants in an urban street canyon—Experimental investigation of the flow and concentration field," Atmos. Environ. **41**, 3287–3302 (2007).

[43]X. Zheng, L. Li, J. Cai, J. Dong, and Q. Li, "Impacts of urban viaducts and noise barriers on traffic pollutant dispersion and residential exposure in the

neighborhood: An analysis using large-eddy simulations," Build. Environ. **285**, 113545 (2025).
[44]X. Zhang, L. Wen, A. U. Weerasuriya, X. Ye, and B. Zhang, "Investigating vehicle effects on wind and pollutant fields in street canyon using the dynamic mesh and source term methods," Sustainable Cities Soc. **130**, 106620 (2025).
[45]B. Zhang, L. Wen, X. Zhang, Y. Fu, T. K. T. Tse, and C. M. Mak, "Enhanced modeling of vehicle-induced turbulence and pollutant dispersion in urban street canyon: Large-eddy simulation via dynamic overset mesh approach," Sustainable Cities Soc. **117**, 105939 (2024).
[46]P. Qin, A. Ricci, and B. Blocken, "On the accuracy of idealized sources in CFD simulations of pollutant dispersion in an urban street canyon," Build. Environ. **265**, 111950 (2024).
[47]C. Gromke and B. Ruck, "Effects of trees on the dilution of vehicle exhaust emissions in urban street canyons," Int. J. Environ. Waste Manage. **4**, 225 (2009).
[48]X. Zheng, H. Montazeri, and B. Blocken, "Large-eddy simulation of pollutant dispersion in generic urban street canyons: Guidelines for domain size," J. Wind Eng. Ind. Aerodyn. **211**, 104527 (2021).
[49]S. Iousef, H. Montazeri, B. Blocken, and P. J. V. van Wesemael, "On the use of non-conformal grids for economic LES of wind flow and convective heat transfer for a wall-mounted cube," Build. Environ. **119**, 44–61 (2017).
[50]E. Sergent, "Vers une méthodologie de couplage entre la simulation des grandes échelles et les modèles statistiques," These de doctorat (Ecole centrale de Lyon, Ecully, 2002).
[51]P. J. Richards and R. P. Hoxey, "Appropriate boundary conditions for computational wind engineering models using the k-ϵ turbulence model," J. Wind Eng. Ind. Aerodyn. **46–47**, 145–153 (1993).
[52]H. Ma, X. Zhou, Y. Tominaga, and M. Gu, "CFD simulation of flow fields and pollutant dispersion around a cubic building considering the effect of plume buoyancies," Build. Environ. **208**, 108640 (2022).
[53]X. Zhou, A. Ying, B. Cong, H. Kikumoto, R. Ooka, L. Kang, and H. Hu, "Large eddy simulation of the effect of unstable thermal stratification on airflow and pollutant dispersion around a rectangular building," J. Wind Eng. Ind. Aerodyn. **211**, 104526 (2021).
[54]D. A. Gerasimov, *Quick Guide to Setting Up LES-Type Simulations, Version 1.4* (European Technology Group, ANSYS Sweden AB, Goteborg, Sweden, 2016).
[55]H. Werner and H. Wengle, "Large-eddy simulation of turbulent flow over and around a cube in a plate channel," in *Turbulent Shear Flows 8*, edited by F. Durst, R. Friedrich, B. E. Launder, F. W. Schmidt, U. Schumann, and J. H. Whitelaw (Springer, Berlin, Heidelberg, 1993), pp. 155–168.
[56]W.-Y. Ng and C.-K. Chau, "A modeling investigation of the impact of street and building configurations on personal air pollutant exposure in isolated deep urban canyons," Sci. Total Environ. **468–469**, 429–448 (2014).
[57]F. Ducros, F. Nicoud, and T. Poinsot, "Wall-adapting local eddy-viscosity models for simulations in complex geometries," Numer. Methods Fluid Dyn. VI **6**, 293–299 (1998).
[58]I. Yimer, I. Campbell, and L.-Y. Jiang, "Estimation of the turbulent Schmidt number from experimental profiles of axial velocity and concentration for high-Reynolds-number jet flows," Can. Aeronaut. Space J. **48**, 195–200 (2002).
[59]F. Bazdidi-Tehrani, S. Masoumi-Verki, P. Gholamalipour, and M. Kiamansouri, "Large eddy simulation of pollutant dispersion in a naturally cross-ventilated model building: Comparison between sub-grid scale models," Build. Simul. **12**, 921–941 (2019).
[60]B. Ji, W. Lei, and Q. Xiong, "An inflow turbulence generation method for large eddy simulation and its application on a standard high-rise building," J. Wind Eng. Ind. Aerodyn. **226**, 105048 (2022).
[61]A. Kubilay, M. K.-A. Neophytou, S. Matsentides, M. Loizou, and J. Carmeliet, "The pollutant removal capacity of urban street canyons as quantified by the pollutant exchange velocity," Urban Clim. **21**, 136–153 (2017).
[62]Y. Tominaga and T. Stathopoulos, "Turbulent Schmidt numbers for CFD analysis with various types of flowfield," Atmos. Environ. **41**, 8091–8099 (2007).
[63]B. Zhou, B. Zhao, X. Guo, R. Chen, and H. Kan, "Investigating the geographical heterogeneity in PM10-mortality associations in the China Air Pollution and Health Effects Study (CAPES): A potential role of indoor exposure to PM10 of outdoor origin," Atmos. Environ. **75**, 217–223 (2013).
[64]T. N. Quang, C. He, L. Morawska, L. D. Knibbs, and M. Falk, "Vertical particle concentration profiles around urban office buildings," Atmos. Chem. Phys. **12**, 5017–5030 (2012).
[65]S. Liu, X. Yang, H. Yang, P. Gao, J. Hang, and Q. Wang, "Numerical investigation of solar impacts on canyon vortices and its dynamical generation mechanism," Urban Clim. **39**, 100978 (2021).